

# Microfluidic Chips for Life Sciences—A Comparison of Low Entry Manufacturing Technologies

*Maximilian Grösche, Ahmed E. Zoheir, Johannes Stegmaier, Ralf Mikut, Dario Mager, Jan G. Korvink, Kersten S. Rabe, and Christof M. Niemeyer\**

**Microfluidic water-in-oil droplets are a versatile tool for biological and biochemical applications due to the advantages of extremely small monodisperse reaction vessels in the pL–nL range. A key factor for the successful dissemination of this technology to life science laboratory users is the ability to produce microfluidic droplet generators and related accessories by low-entry barrier methods, which enable rapid prototyping and manufacturing of devices with low instrument and material costs. The direct, experimental side-by-side comparison of three commonly used additive manufacturing (AM) methods, namely fused deposition modeling (FDM), inkjet printing (InkJ), and stereolithography (SLA), is reported. As a benchmark, micromilling (MM) is used as an established method. To demonstrate which of these methods can be easily applied by the non-expert to realize applications in topical fields of biochemistry and microbiology, the methods are evaluated with regard to their limits for the minimum structure resolution in all three spatial directions. The suitability of functional SLA and MM chips to replace classic SU-8 prototypes is demonstrated on the basis of representative application cases.**

## 1. Introduction

Droplet microfluidics is an increasingly important technology that addresses a broad range of applications in the (bio)chemistry and life sciences, such as nanoparticle synthesis,<sup>[1]</sup> (digital) PCR,<sup>[2]</sup> or single-cell analysis.<sup>[3]</sup> The miniaturization of conventional reaction vessels into single water-in-oil (W/O) droplets realized in such applications leads to a considerable reduction of the reaction volume, which, in turn, minimizes the required sample and reagent consumption and leads to better control over temperature and diffusion-based

mixing. These features can often accelerate or even enable reactions to proceed.<sup>[4]</sup> A key factor for the successful dissemination of this technology is the ability for production of masters for molding microfluidic droplet generators and related accessories through rapid prototyping with low associated manufacturing and material costs, because only few ready-to-use microfluidic devices are currently commercially available and their geometries are usually limited to standard applications.

Soft lithography using SU-8 masters is the gold standard for the production of microfluidic prototypes.<sup>[5]</sup> In this method, an SU-8 photoresist is structured by means of optical lithography and the resulting negative structure is then molded by soft lithography into polydimethylsiloxane (PDMS). For sealing, the elastomeric PDMS chips are usually plasma bonded onto glass supports. The very high structural resolution along with excellent surface

quality in terms of low roughness is the major advantages of this technology, whereas low aspect ratios and difficulties in the production of variable heights in a single chip, along with high machine costs and the requirement of clean room facilities for the production of masters, are on the downside. Since trained clean room personnel and expensive infrastructure are often not available in research institutes engaged in biomedical research and the life sciences, there is a great demand for alternative cost-effective manufacturing processes for microfluidic chips.

The implementation of additive manufacturing (AM) methods in microfluidic prototyping is currently attracting

---

M. Grösche, A. E. Zoheir, Dr. K. S. Rabe, Prof. C. M. Niemeyer  
Karlsruhe Institute of Technology (KIT)  
Institute for Biological Interfaces (IBG 1)  
Hermann-von-Helmholtz-Platz 1, D-76344 Eggenstein-Leopoldshafen,  
Germany  
E-mail: niemeyer@kit.edu  
Dr. J. Stegmaier  
RWTH Aachen University  
Institute of Imaging and Computer Vision  
Kopernikusstraße 16, 52074 Aachen, Germany

Prof. R. Mikut  
Karlsruhe Institute of Technology (KIT)  
Institute for Automation and Applied Informatics (IAI)  
Hermann-von-Helmholtz-Platz 1, D-76344 Eggenstein-Leopoldshafen,  
Germany  
Dr. D. Mager, Prof. J. G. Korvink  
Karlsruhe Institute of Technology (KIT)  
Institute of Microstructure Technology (IMT)  
Hermann-von-Helmholtz-Platz 1, D-76344 Eggenstein-Leopoldshafen,  
Germany

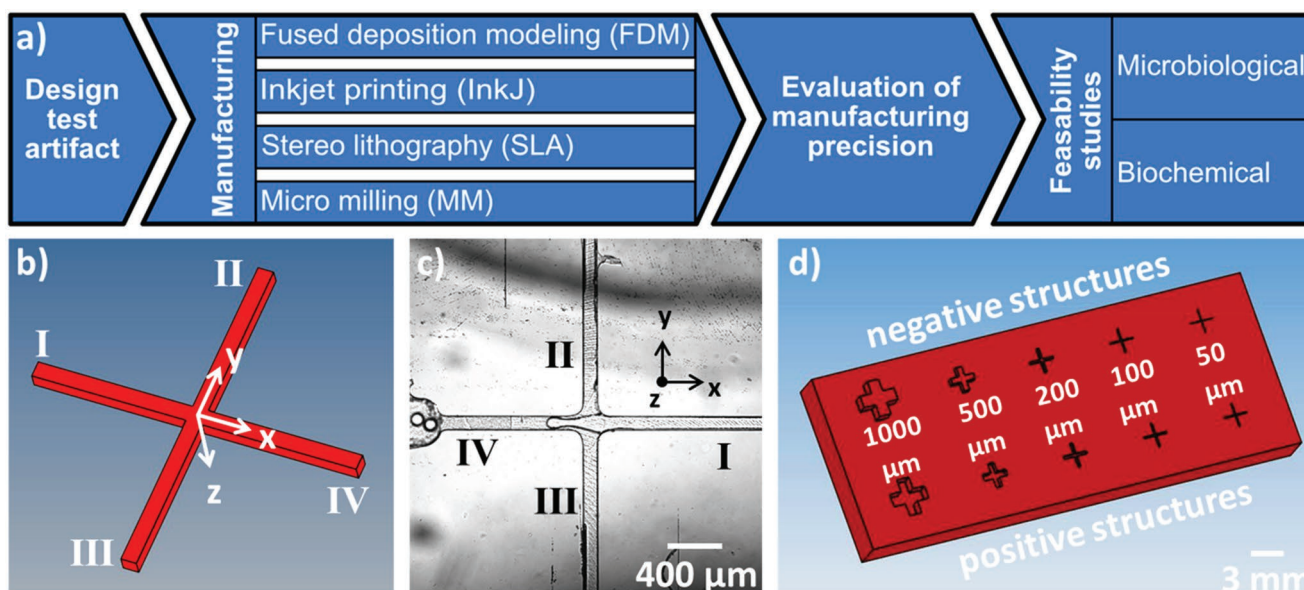


**Figure 1.** a) Process-diagram for the comparison of the manufacturing techniques. b) Schematic illustration of the test artifact used for the evaluation of additive manufacturing methods. The structure of the artifact corresponds to that of c) a flow focusing structure with one inlet for the dispersed phase (I), two inlets for the continuous phase (II, III), and one outlet (IV). Z-axis represents the depth of the structure, X and Y axes the widths in Y and X directions, respectively. d) Test artifact with positive (recessed) and negative (elevated) structures, having an aspect ratio of 1:1 with widths of 1000, 500, 200, 100, and 50  $\mu\text{m}$ .

much attention because AM is associated with low machine and operating costs, simple handling, and high flexibility.<sup>[6]</sup> Commonly used AM methods include technologies, such as fused deposition modeling (FDM), inkjet printing (InkJ), and stereolithography (SLA), all of which are nowadays offered by commercial “print shops” that produce devices on-demand for non-expert users. In the academic community, AM for microfluidic applications is under extensive development.<sup>[7]</sup> Devices with structures  $>500 \mu\text{m}$ , such as supports, racks, and other laboratory accessories, or millifluidic chips can be conveniently produced by AM.<sup>[8]</sup> Specialized groups have reported on 3D printed microfluidic structures with structure sizes of  $\geq 400\text{--}500 \mu\text{m}$ . Examples include microfluidic mixers,<sup>[9]</sup> multimaterial chips for measuring pharmaceuticals,<sup>[10]</sup> or embedded membrane chips for colorimetric analysis.<sup>[11]</sup> Likewise, 3D printed droplet generators have been reported to enable production of droplets with diameters of  $300\text{--}500 \mu\text{m}$  using flow rates ranging from some  $100 \mu\text{L min}^{-1}$ <sup>[12]</sup> to the  $\text{mL min}^{-1}$  regime.<sup>[13]</sup>

The above structure sizes can be reduced substantially by sophisticated instrumentation,<sup>[14]</sup> printing materials,<sup>[15]</sup> and process-engineering.<sup>[16]</sup> Cutting edge examples of structures  $<100 \mu\text{m}$  include 3D printed support structures for metal cannulas<sup>[17]</sup> or tubes,<sup>[18]</sup> free-flow electrophoresis chips,<sup>[19]</sup> droplet generators,<sup>[20]</sup> or even devices bearing features in the  $<20 \mu\text{m}$  regime.<sup>[14,21]</sup> While comparisons between manufacturing processes describe minimum achievable structural resolutions for experienced, specialized groups,<sup>[22]</sup> the practical relevance for research groups from the life sciences often remains unclear. Therefore, to evaluate AM processes for typical microfluidic life science applications, such as microbiological and biochemical experiments in microfluidic droplets, we report here on the direct, experimental side-by-side comparison of three

commonly used AM methods, FDM, InkJ and SLA, all of which are accessible through commercially available instruments and services. As a benchmark in this comparison, we used micro-milling (MM) as an established method with a low entry barrier. The four manufacturing methods were evaluated with regard to their limits for the minimal structure resolution in all three spatial directions. Selected methods were used as molds for production of prototype microfluidic devices by PDMS soft lithography to utilize the advantages of this elastomeric material in terms of biocompatibility, low autofluorescence, and well-established surface coating techniques. Representative case studies on the encapsulation of bacteria and the investigation of enzyme kinetics in droplets indicate that SLA and MM can replace classical SU-8 prototyping for the production of functional chips (Figure 1).

## 2. Results

### 2.1. Evaluation of Manufacturing Precision

Since the various test structures suggested for evaluation of additive manufacturing processes<sup>[23]</sup> and milling machines<sup>[24]</sup> differ largely in size and structural complexity, we chose a single cross-shaped test artifact whose size was varied (Figure 1).

It represents the typical design of a flow-focusing intersection used for generating water-in-oil (W/O) droplets and, thus, is of high relevance for real-life applications in the biomedical sciences. The precise fabrication of a flow-focusing intersection is essential for adjustment of droplet size<sup>[25]</sup> and a high contour accuracy is paramount for the proper functioning

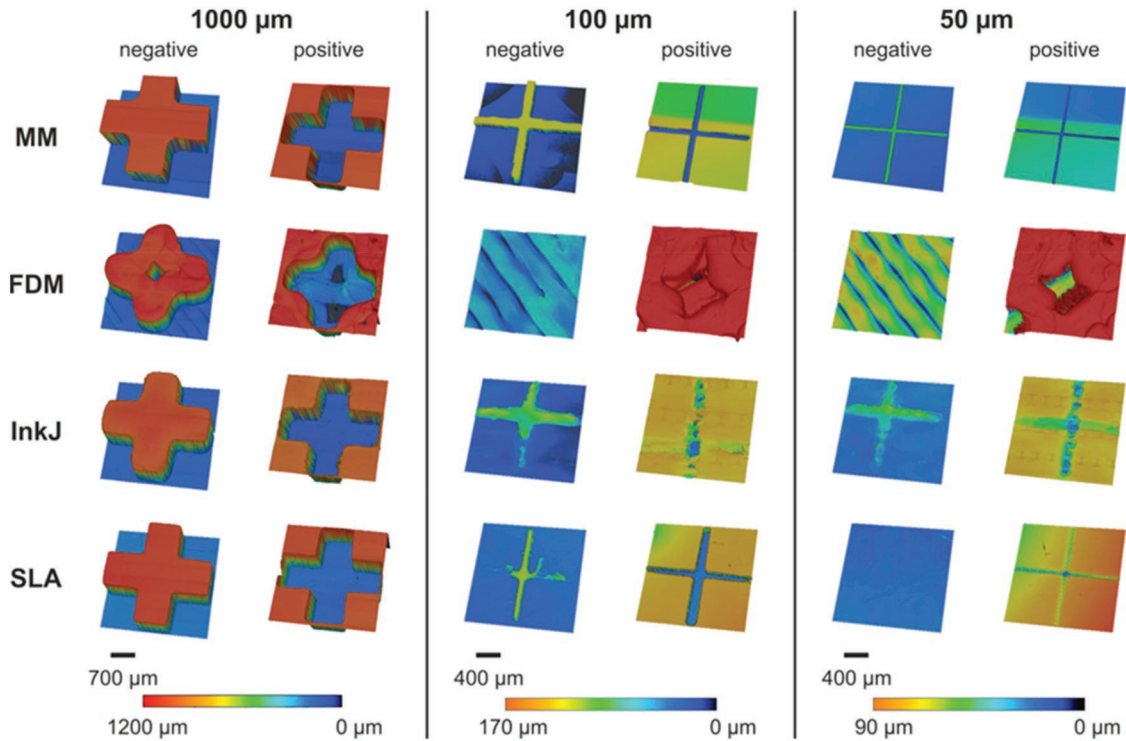


**Figure 2.** 3D representations of the confocal images of the test structures. Structures with 1000, 100, and 50  $\mu\text{m}$  in width and height are shown as negative and positive structures. Each row shows the results from a particular manufacturing technology. MM, micromilling; FDM, fused deposition modeling; InkJ, inkjet printing; and SLA, stereo lithography. The depth of the structures is represented by color coding.

of microfluidic structures. Our cross-shaped test artifact was designed in accordance with guidelines from the National Institute of Standards and Technology (NIST, USA),<sup>[26]</sup> specifying that test artifacts should contain sufficiently small and large structures, and they should additionally consist of elevated and recessed structures. Further, the structures should be designed such that they can be produced in short times and consume only small amounts of material.

**Figure 2** shows representative confocal images of the test structures produced with all four manufacturing techniques. The 50 and 100  $\mu\text{m}$  structures shown represent design dimensions most frequently used in droplet microfluidics. Since not all AM techniques were capable of producing structures with this resolution, the 1000  $\mu\text{m}$  geometry structures are shown for comparison. The results obtained for the corresponding 500 and 200  $\mu\text{m}$  geometries are included as numerical values in **Figure 3**. Confocal image analysis showed that all structures down to the minimum resolution of 50  $\mu\text{m}$  could be produced in high quality by MM with no obvious differences between negative and positive structures. In contrast, FDM was not suitable to produce any of the desired structures. In agreement with an earlier study revealing the limited resolution of FDM,<sup>[27]</sup> even the 1000  $\mu\text{m}$  structure showed only a rough approximation to the desired form, with strongly rounded edges and a hole in the negative structure, as well as missed shape and position tolerances in the positive structures.

The use of InkJ enabled production of the 1000  $\mu\text{m}$  structures nearly as well as with MM. The 100 and 50  $\mu\text{m}$  negative structures showed the basic features, however, they were far

removed from the geometry of the target. The positive structures could not be manufactured at all. SLA enabled a better reproduction of the target structures. However, the negative 100  $\mu\text{m}$  structure was found to have insufficient mechanical stability as it was damaged already in the initial washing step that preceded the PDMS molding process. Although the positive structures were in the correct size range, the cross junction was inhomogeneous in width. The 50  $\mu\text{m}$  negative structure could not be manufactured by SLA and the corresponding positive structure was largely incomplete.

## 2.2. Comprehensive X–Y–Z Characterization

To allow for a quantitative comparison of the manufacturing methods, all structures were first characterized by confocal microscopy analysis with regard to channel width and depth. **Figure 3** shows the measured lateral and vertical structure size in comparison to the target values (dashed line). It is evident that the AM methods revealed a general weakness in the production of lateral features  $\leq 200 \mu\text{m}$ . With the FDM and InkJ processes, positive (recessed) features were produced more accurately than negative (elevated) ones. Also there is a tendency for positive features to be smaller, while negative ones are larger in lateral size. SLA behaves inversely and the data revealed only small differences in the precision of the X- and Y-axes, with a higher precision for the Y-axis.

While MM could resolve both negative and positive structures well down to the 50  $\mu\text{m}$  lateral resolution limit tested,

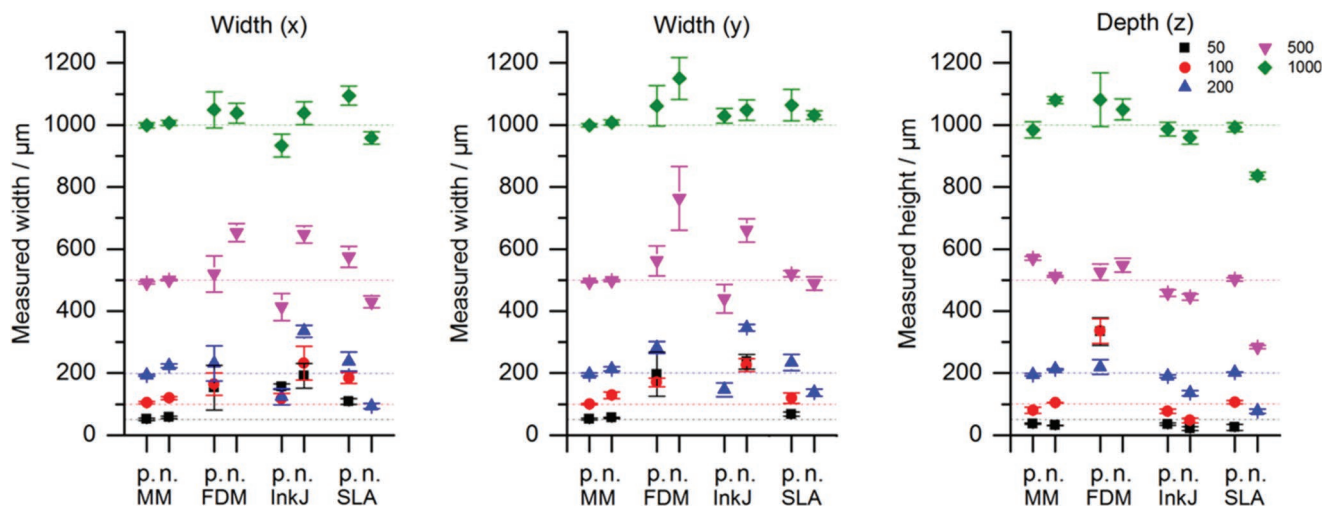


**Figure 3.** Comparison of experimentally determined structure sizes with the corresponding target values of the model. The structure widths in the x-, y-, and z-directions are plotted against the target values (dotted lines). p: positive (recessed) structure; n: negative (elevated) structure.

heterogeneous results were obtained for the AM methods. Substantial deviations from the target dimensions indicated that SLA and InkJ showed an average lateral resolution limit of about 350  $\mu\text{m}$ . The vertical resolution, however, was sufficient to resolve structure depths down to 200  $\mu\text{m}$  for all methods except SLA, the latter of which was not capable of printing negative structures.

Due to the availability of commercial 3D printers, the FDM process is the most commonly used method because it is comparatively robust and fast, to allow for manufacturing of parts in short times. However, our results suggest that FDM is not well suited for the fabrication of microfluidic structures. This is in line with the report of Salentijn et al.,<sup>[27]</sup> who evaluated FDM manufacturing of rectangular and round structures down to 1 mm lateral size. Kitson et al.<sup>[8a]</sup> have shown that microfluidic experiments are possible in FDM-based structures, even when the resolution limit was only about 800  $\mu\text{m}$ . King et al.<sup>[28]</sup> reported that microstructured droplet generators could be manufactured by FDM, however, only very large droplets with diameters in the millimeter range were produced. Hence, the FDM method seems well suited for production of millifluidic components with larger volume requirements or laboratory accessories.

InkJ and SLA processes showed a satisfactory resolution in the manufacturing of 3D components with lateral dimensions in the range of 200–500  $\mu\text{m}$ . With the average resolution observed here of about 350  $\mu\text{m}$ , these processes can be a good alternative to the classic SU-8 or the MM processes. Comparative assessments of AM methods for microfluidic application are rare,<sup>[6b,8c,29]</sup> and reports usually focus on one or two particular processes. However, representative examples clearly indicate that the resolution limit of these methods is in the range of 300  $\mu\text{m}$ ,<sup>[6,30]</sup> thus confirming the results obtained in our study, which also emphasizes the utility of MM, revealing a resolution limit of  $\leq 50$   $\mu\text{m}$  in both the lateral and vertical dimensions. This satisfactory resolution clearly compensates the increased effort in model preparation by CAD-CAM transfer that is required for MM manufacturing.

### 2.3. Real-Time Analysis of Bacteria in Microfluidic Droplets

Since the above study identified the SLA and MM processes as best suited for the production of miniaturized structures, we used these methods to produce molds for soft lithography manufacturing of prototype microfluidic devices for typical biochemical and microbiological applications. As a first case, we chose the encapsulation of microbial cells inside microfluidic W/O droplets. This approach is considered a key enabling technology for future applications in microbiology and biotechnology,<sup>[31]</sup> because it enables detailed cell studies with a tunable resolution ranging from small cell populations to the single-cell level along with high sensitivity and precision, ultra-high-throughput, and reduced consumption of expensive media and reagents. Recent examples include the evolution of enzyme expressing recombinant *Escherichia coli* cells, using either fluorescent<sup>[32]</sup> or absorbance-based<sup>[33]</sup> assays, the screening of environmental metagenomic samples for new enzymes,<sup>[34]</sup> or screening of industrially improved strains for metabolite production and substrate conversion.<sup>[35]</sup> Such studies underline the enormous potential of microfluidic droplet technology, which could be further advanced by the development of low-cost additive manufacturing processes.

To elaborate on this perspective, we designed microfluidic test structures consisting of a flow-focusing intersection and a droplet storage chamber (**Figure 4**), which were manufactured either by SLA or MM to realize minimal structure sizes of 350 or 100  $\mu\text{m}$ , respectively. Employing 1  $\mu\text{L min}^{-1}$  as the standard flow rate, droplets with a typical diameter of 560 or 130  $\mu\text{m}$ , respectively, were generated in the SLA or MM chips, corresponding to volumes of about 92 or 1.2 nL, respectively. This means that for the generation of 1000 droplets with the SLA structure about 90  $\mu\text{L}$  sample are required, whereas the MM structure only needs 1  $\mu\text{L}$ . Even though the flow rate of the continuous phase in the SLA structure was increased by a factor of 20, the concurrent decrease in droplet size to about 400  $\mu\text{m}$ , still required substantially more specimen samples and flow media in comparison to the smaller 130  $\mu\text{m}$  droplets generated by the MM chip.

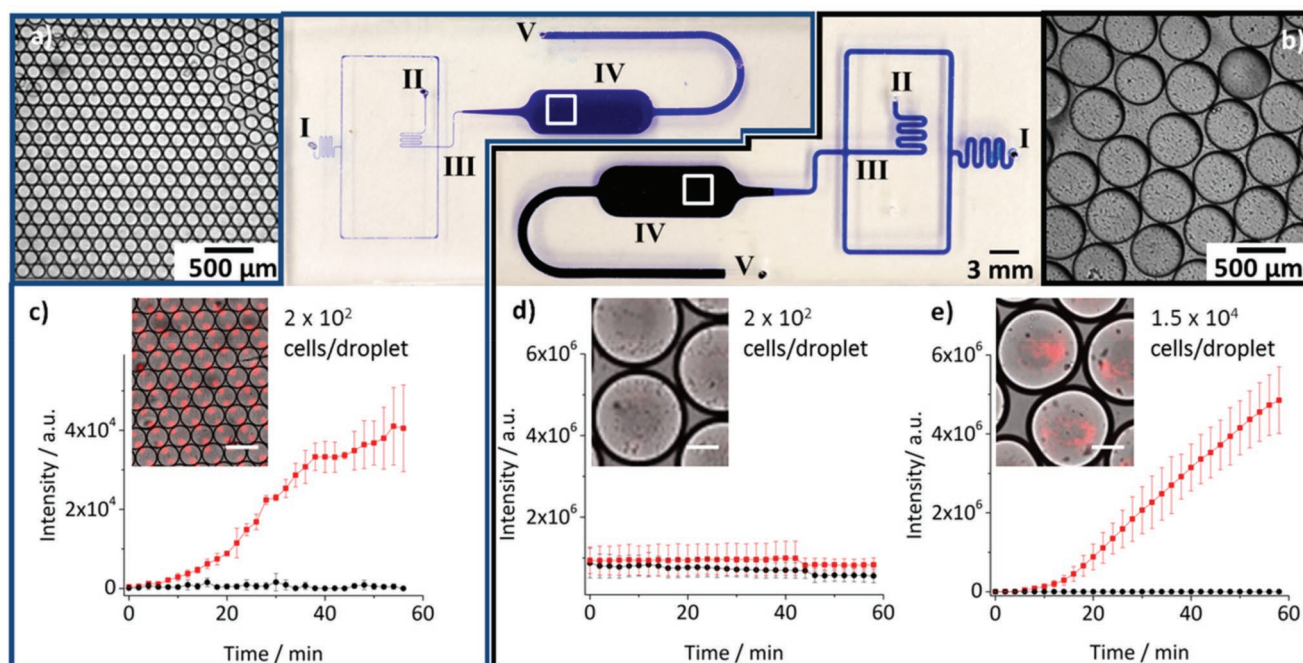


**Figure 4.** Microfluidic chip manufactured by a) MM or b) SLA, both of which contained an oil inlet (I), an aqueous phase inlet (II), the flow focusing intersection (III) for droplet generation, an OCS chamber (IV), and an outlet (V). The inset images show detailed views of the OCS containing W/O droplets with encapsulated *E. coli*. The graphs in c) (MM) and d–e) (SLA) depict time-dependent fluorescent signals originating from the expression of RFP after induction of *E. coli* cells with arabinose (red), whereas the negative controls (black) lack arabinose. Droplets were loaded with variable numbers of *E. coli* cells. The insets show magnified images of droplets. Note that no substantial signal was detectable when the number of cells was too small in relation to the droplet volume (d). Also note that the threshold required for image acquisition had to be adjusted individually for each experiment to the intensity of the bacterial fluorescence signals at time  $t = 0$ , thus leading to differences in the absolute fluorescence intensity. Scale bars are 200  $\mu\text{m}$ . Error bars represent at least experimental duplicates.

In the first set of experiments, a constant number of about 200 *E. coli* cells, bearing the red fluorescent protein (RFP) encoding pAra-mRFP1 vector, were encapsulated in W/O droplets using either the MM or SLA chip. Expression of RFP inside the droplets was monitored in real time over 60 min and analyzed using the in-house developed MATLAB software. We observed an initial phase of about 15 min with slow increase in fluorescence (Figure 4c), which reflects the time of handling (10 min off chip) as well as the initial on-phase of mRNA transcription, protein biosynthesis, and folding, similar as previously observed by others.<sup>[36]</sup> Subsequently, an exponential signal increase of about 30 min occurred, indicating the continuous protein production phase, after which the signal increase receded due to decreasing amounts of nutrients, which slow down protein expression and cell growth.

Next, the suitability of the SLA chip was tested by producing W/O droplets that contained the same cell number as set in the MM droplets (Figure 4d). To this end, the cell density in the dispersed phase was decreased from  $\approx 1.6 \times 10^5 \text{ cells } \mu\text{L}^{-1}$ , used for generation of MM droplets, to  $\approx 2000 \text{ cells } \mu\text{L}^{-1}$  because of the increased volume of the SLA droplets. Despite the same droplet loading, no satisfactory signal generation could be observed (Figure 4d). Owing to the spatial distribution of cells in the larger droplet volume, too few cells are located in the focal plane of the microscope, resulting in an insufficiently bright fluorescence signal. Hence, in order to confirm the general suitability of the SLA chip for this type of application, the cell density in the

dispersed phase was increased to  $1.6 \times 10^5 \text{ cells } \mu\text{L}^{-1}$  (Figure 4e), similar to that used for droplet generation in the MM chip. Indeed, the resulting droplets containing about  $1.5 \times 10^4$  cells per droplet showed a comparable signal progression with the signal amplitude in the larger SLA droplets resembling that of the smaller MM droplets (compare Figure 4c,e). The results thus indicate that the encapsulation of cells in W/O drops can be performed in both structures. However, the SLA structure shows disadvantages, due to higher reagent consumption upon generation of the larger droplets, and because larger numbers of cells need to be encapsulated to ensure proper read-out.

#### 2.4. Enzyme Kinetics Inside Microfluidic Droplets

In addition to cell encapsulation, the kinetic characterization of enzymes constitutes another important field of applications for microfluidic droplet technology.<sup>[37]</sup> Since enzyme kinetics usually requires defined mixtures of enzymes and substrates, we designed a microfluidic chip that consists of an inlet for the continuous phase (I, in Figure 5a) and two inlets (II, III) for two disperse phases to be mixed.

At junction IV, the two disperse phases are combined and encapsulated in the oil phase, then pass the mixer structure (V), to be collected in the storage chamber (VI, Figure 5a). Chips for these experiments were again manufactured by using either the MM or the SLA method.

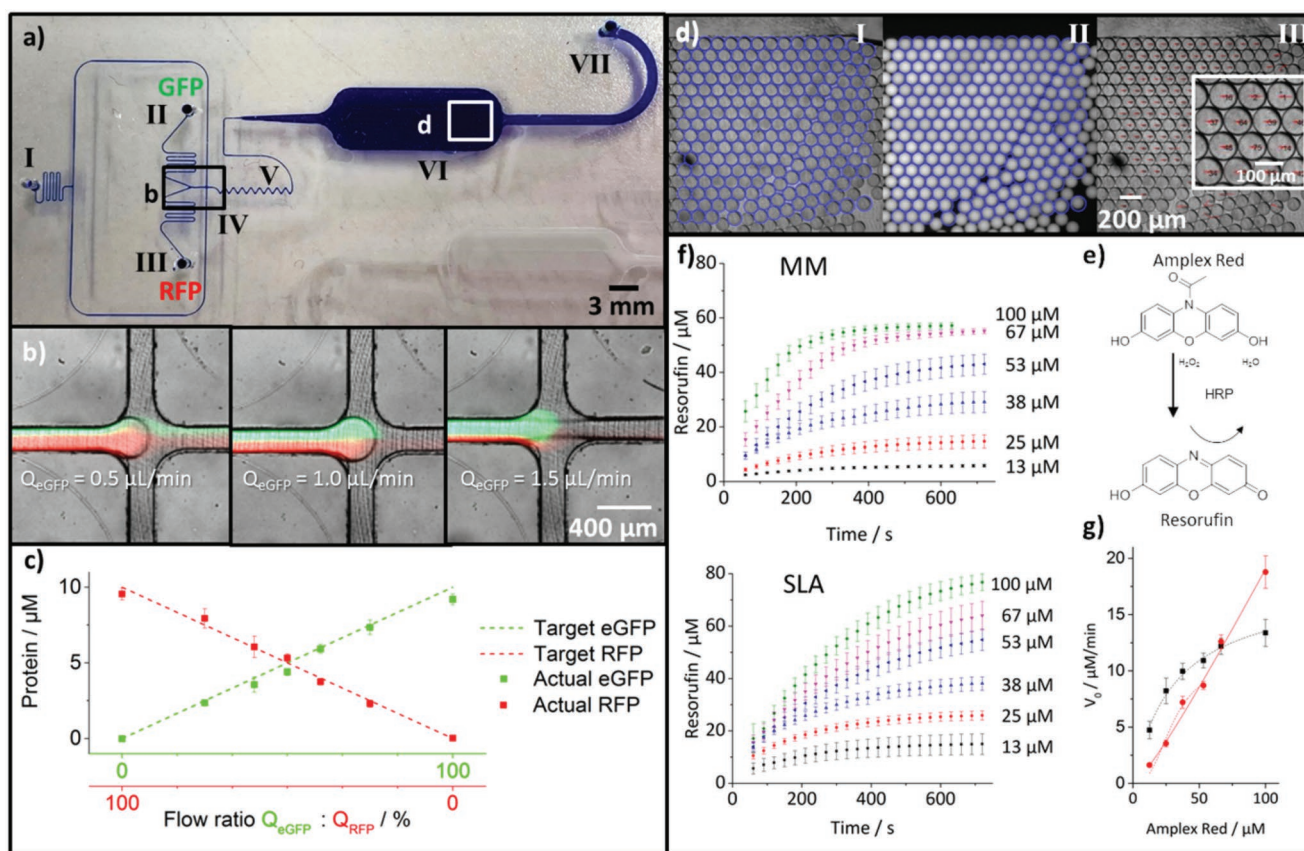


**Figure 5.** a) Microfluidic mixer combined with a W/O droplet generator chip for enzyme kinetics, manufactured by MM. I is the inlet for the continuous oil phase. Two disperse phases, injected through inlets II, III are mixed by difference in their flow rates before they are encapsulated into droplets in section IV. Section V is a fluidic mixer that promotes diffusion-based mixing of encapsulated reagents. VI is the OCS chamber and VII is the outlet. b) Representative superimposed fluorescence images showing the mixture of GFP and RFP solutions at the given volume ratio, determined by the respective flow rates applied to inlets II and III. c) Calculated (dashed line) and experimentally determined (data points) GFP/RFP protein concentrations in the droplet as a function of flow rate ratio during encapsulation. d) Representative micrographs obtained during automated droplet analysis showing droplet detection in the reflected image (I), center superimposition of positional data on fluorescence image and measurement of intensity per droplet (II) and motion trajectories of droplets (III). e) HRP-catalyzed conversion of fluorogenic substrate Amplex Red to Resorufin. f) Time course development of Resorufin production, measured via fluorescence intensity in droplets generated in the MM (top) and SLA (bottom) chips at different Amplex Red concentrations. g) Dependence of reaction rates  $V_0$  on the initial Amplex Red concentration, determined in droplets generated in the MM (red circles) and SLA (black squares) chips. Curve fitting using Hill equation was applied to calculate the  $K_m$  values. Error bars show mean of at least 30 Droplets per experiment.

In a first set of experiments, the mixing capability of the chip was characterized by merging two aqueous solutions containing either green or red fluorescent protein (GFP, RFP) in the same concentration, of which defined volume fractions were injected into the droplets by adjusting the flow rate ratio applied to inlets II and III. As expected, this led to formation of droplets containing mixtures of GFP/RFP with the desired protein concentrations (Figure 5b,c). The obtained concentration ratios were experimentally determined by fluorescence microscopy and semiautomated image analysis using the in-house developed algorithm for droplet identification, tracking, and fluorescence intensity calculation.<sup>[38]</sup> Results are depicted in Figure 5d, where the blue circles indicate the droplet boundaries identified by the software (image I, in Figure 5d). These boundaries are projected onto the fluorescence images to determine the fluorescence intensities inside a given droplet (II, in Figure 5d). Each droplet is tracked by a nearest neighbor

method throughout the duration of the entire experiment. An example of this motion trajectory is shown in image III (Figure 5d).

Having shown that the microfluidic chip was capable to generate W/O droplets with precisely adjusted volume ratios of two components, the set-up was used to evaluate the performance of the MM and SLA structures for the analysis of droplet confined enzyme kinetics. To this end, we chose the well-established conversion of the non-fluorescent Amplex Red substrate into the highly fluorescent product resorufin, which is catalyzed by horseradish peroxidase (HRP) in the presence of hydrogen peroxide (Figure 5e). The resulting data (Figure 5f) were used for the calculation of reaction rates that were plotted against the substrate concentration (Figure 5g). In case of the SLA Chip the  $V_0/[S]$  graph showed the expected plateau toward higher substrate concentrations, thus leading to an

estimated Michaelis-Menten constant ( $K_m$ ) of  $31 \times 10^{-6}$  M, which is lower than the  $K_m$  values obtained from microplate experiments ( $K_m \approx 100\text{--}200 \times 10^{-6}$  M).<sup>[39]</sup> Interestingly, the reaction in the smaller MM droplets occurred substantially faster, as clearly indicated by the truncation of the initial phase of signal development (Figure 5f) as well as by the linear slope of the  $V_0/[S]$  plot, which does not reach the expected plateau within the concentration range employed. Taken together, these results suggest that the reaction velocity of the relatively complex two-step enzymatic oxidation of Amplex Red is strongly dependent on the droplet size. This is in line with investigations to influence a much simpler, uncatalyzed bimolecular reaction by the altered surface/volume ratio of differently sized W/O droplets.<sup>[40]</sup>

### 3. Conclusion

Our comparative evaluation of cost-effective manufacturing processes for microfluidic droplet applications shows that AM methods can indeed be competitive to established MM and SU-8 lithography. While SLA showed the best structural resolution of the AM methods (about  $350 \mu\text{m}$ ), it is still substantially lower than MM ( $<50 \mu\text{m}$ ). This means that the droplet generators manufactured with SLA must be approximately five times larger to obtain functional structures. This leads to significantly larger droplets and thus to a substantially higher consumption of sample solutions and reagents. Depending on the biological application, the increased volume requirement may be tolerable, for example, if inexpensive enzymes and substrates are to be characterized. However, when it comes to expensive, valuable components such as delicate enzymes or rare cells, systems with low-volume requirements are clearly advantageous. The smaller reaction space also has a positive effect on optical analytics, as we have shown here with the example of encapsulated *E. coli* cells. Since MM is currently offering the largest flexibility in terms of structure size and complexity, we conclude that this method is currently best suited for the rapid prototyping and manufacturing of microfluidic droplet generator chips.

However, since AM methods have principle advantages, for example, in their ability to create multilayer functional units by adding sacrificial materials, the current rise of refined methodologies,<sup>[14–21]</sup> and in particular, the two-photon polymerization (2PP) and direct laser writing techniques (DLW),<sup>[41]</sup> promise substantially improved resolution ( $<10 \mu\text{m}$ ) with a concomitant reduction in writing times and costs. Since the development of 2PP and DLW continues to progress analogously to the low-entry 3D printing processes considered here, and they will become more cost-effective and more widely available, even highly complex microfluidic structures will be much easier to access in the future. Thus it is foreseeable that single-stage production processes involving multi-material printing will become possible, for example, to produce completely closed, chemically inert microstructures with integrated electrodes by using AM methods, without numerous process steps being necessary. The fabrication of such complex structures in a single printing process should allow it to make complex microfluidic applications, such as the sequential fusion of triple-core double emulsions

triggered by electric fields,<sup>[42]</sup> more easily accessible to a broad range of users.

### 4. Experimental Section

*Evaluation of Manufacturing Precision:* To evaluate manufacturing precision, a cross-shaped structure was used (Figure 1a) that is based on the typical design of a flow-focusing intersection (Figure 1b) containing an inlet (I) for the dispersed (aqueous) phase, two perpendicularly arranged inlets (II, III) for the continuous (oil) phase, and an outlet (IV). The artifact (Figure 1c) consisted of elevated (negative) and recessed (positive) structures, each with a width in the  $x$  and  $y$  directions of, respectively, 1000, 500, 200, 100, or  $50 \mu\text{m}$ . The aspect ratio of all structures was 1:1. The test artifact was designed using CAD (computer-aided design, Inventor 2018, Autodesk). For micromilling, the construction file was translated to machine code using the built-in CAD-CAM transfer (HSM Inventor Pro, Autodesk). The structure was then produced by micromilling (Mini Mill GX, Minitex Machinery, US) of a polymethyl methacrylate (PMMA, Evonik Industries) block. The largest possible milling tool (HAMPP Tools, Germany) was used for each structure.

For the evaluation of 3D printing procedures, the structure was converted into STL-files and manufactured by fused deposition modeling from acrylonitrile-butadiene-styrene copolymer on a Designjet Color 3D (Hewlett Packard), by inkjet printing of “Verowhite” polymer with a Eden260V plotter (Stratasys), or by stereolithography with the BV-003 polymer on a MiiCraft+ device (MiiCraft). The subsequent cleaning was carried out in accordance with the manufacturer’s instructions. All structures were then characterized for their geometry, shape tolerance and surface roughness by using a Keyence VK-X Laser Scanning Microscope. To this end, the entire geometry was measured in a high resolution mode with a  $z$ -pitch of  $200 \text{ nm}$ . The images were taken with a  $20\times$  lens. The contour accuracy in terms of lateral and vertical resolution was measured at 10 points evenly distributed over the intersection.

*Microfluidic Water-in-Oil Droplet Applications:* The two structures manufactured by MM and SLA were tested for their performance in biochemical and microbiological applications. Two established model applications of microfluidic water-in-oil (W/O) droplet technology were chosen. For this purpose, two types of microfluidic chips were manufactured. The first type was designed for the encapsulation of microorganisms in W/O droplets to enable their time-resolved investigation inside an on-chip storage (OCS) chamber. The other type was designed for droplet-based high-throughput enzyme assays. Schematics of the two chips are shown in Figures 4 and 5, respectively. The master structures for soft lithography molding were produced either by MM (Figure 4a) or SLA (Figure 4b). Therefore, the dimensions of the flow focusing junctions were determined by the minimum structure resolution of the respective method. As detailed above, these corresponded to  $350$  or  $50 \mu\text{m}$  for SLA and MM, respectively. Both masters were molded with PDMS (Sylgard 184, Dow Corning) in a standard soft lithography process. The PDMS prepolymer and curing agent were mixed in a ratio of 10:1 and the polymer was poured into the mold and degassed for 30 min. After curing at  $70 \text{ }^\circ\text{C}$  for 3 h, the inlets were punctured with a biopsy needle ( $D = 1 \text{ mm}$ ) and the PDMS was sealed with a glass slide using plasma bonding. The microfluidic chips were then connected to a syringe pump system (neMESYS, Cetoni, Germany) using standard PTFE tubing.

*E. coli* DH5 $\alpha$  cells were transformed with a pAra-RFP plasmid to enable the expression of Red Fluorescent Protein (RFP) upon exposure to arabinose containing medium. The arabinose regulatory element pAra was amplified by PCR using the pTF16 vector (Takara Bio Inc., Japan) as a template and inserted into a lab stock pMK vector (GeneArt, Thermo Scientific, Germany, containing the RFP variant mRFP1) by Gibson isothermal assembly.<sup>[43]</sup> The vector was transformed into chemically competent *E. coli* DH5 $\alpha$  cells and successful cloning was verified

by commercial sequencing (LGC genomics, Germany). The bacteria were grown overnight and, shortly before microfluidic encapsulation, diluted to 160 000 cells  $\mu\text{L}^{-1}$  with LB medium containing  $10 \times 10^{-3}$  M arabinose. The flow rate of the dispersed phase for the encapsulation of the bacteria was  $Q_{\text{disp}} = 1 \mu\text{L min}^{-1}$ . Fluorocarbonated oil (BioRad Droplet Generation Oil) with a flow rate  $Q_{\text{cont}} = 12 \mu\text{L min}^{-1}$  was used as the continuous phase. Bacterial expression of RFP from the pAra-RFP plasmid was quantitatively determined by fluorescence microscopy (Zeiss Observer, Zeiss; Prime 95B camera, Photometrix).

For determination of enzyme kinetics inside W/O droplets, the horseradish peroxidase (HRP) catalyzed conversion of the fluorogenic substrate Amplex Red to resorufin was used. The reaction partners were injected into W/O droplets as two separate phases that were joined together at the droplet generation junction. One phase  $Q_{\text{disp-1}}$  consisted of HRP (type VI, Sigma, 4 mU),  $400 \times 10^{-6}$  M hydrogen peroxide (Sigma) in  $100 \times 10^{-3}$  M TRIS buffer (pH 8.1). The other phase  $Q_{\text{disp-2}}$  consisted of HRP (type VI, Sigma, 4 mU),  $133 \times 10^{-6}$  M Amplex Red (Invitrogen) and  $100 \times 10^{-3}$  M TRIS buffer (pH 8.1). Variable concentrations of Amplex Red in the droplets were adjusted, by modulating the ratio of the two flow rates  $Q_{\text{disp-1}}:Q_{\text{disp-2}}$  while keeping the total flow rate constant ( $Q_{\text{disp-1}} + Q_{\text{disp-2}} = 2 \mu\text{L min}^{-1}$ ). The continuous flow rate for encapsulation was  $Q_{\text{cont}} = 12 \mu\text{L min}^{-1}$ .

Droplets generated in this way were collected as a monolayer inside the OCS chamber to facilitate quantitative assessment of fluorescent signals. Signal detection was realized by fluorescence microscopy imaging, combining a reflected light (Figure 5d) and a fluorescence image. The two images were merged by an in-house developed algorithm that allowed tracking of individual droplets with algorithms previously described.<sup>[38a]</sup> The software processed series of 2D images to determine temporal changes in fluorescence intensity inside the droplets. To this end, droplets were automatically detected separately in each frame. The graphical user interface allowed for semiautomated rejection of erroneous structures and objects touching the chamber's border regions to prevent incorrect measurements of incomplete or disappearing objects. Droplet locations were tracked using a nearest neighbor tracking algorithm that linked each object to its spatially nearest neighbor in the next frame. Only tracks covering the entire time interval were used for further analysis. The results of the detection and tracking can be exported to CSV files and videos. All algorithms are implemented in MATLAB and the tracking algorithm is based on the implementation that comes with SciXMiner.<sup>[38b]</sup> The code is available under the GNU-GPL v3 license under <https://github.com/stegmaierj/dropletanalysis/tree/master/DropletAnalysis/>.

## Acknowledgements

This work was supported by the Helmholtz programme "BioInterfaces in Technology and Medicine." The authors thank Teresa Burgahn for providing the reagents for the enzyme kinetics and fruitful discussions. The authors thank Jörg Bohn and Jonas Wohlgemuth for printing the test artifacts.

## Conflict of Interest

The authors declare no conflict of interest.

## Keywords

additive manufacturing methods, cells, enzyme kinetics, microfluidics, microstructures

- [1] a) I. Shestopalov, J. D. Tice, R. F. Ismagilov, *Lab Chip* **2004**, *4*, 316; b) R. Galinis, G. Stonyte, V. Kiseliovas, R. Zilionis, S. Studer, D. Hilvert, A. Janulaitis, L. Mazutis, *Angew. Chem., Int. Ed.* **2016**, *55*, 3120; c) V. B. Varma, R. G. Wu, Z. P. Wang, R. V. Ramanujan, *Lab Chip* **2017**, *17*, 3514.
- [2] a) M. M. Kiss, L. Ortoleva-Donnelly, N. R. Beer, J. Warner, C. G. Bailey, B. W. Colston, J. M. Rothberg, D. R. Link, J. H. Leamon, *Anal. Chem.* **2008**, *80*, 8975; b) D. Pekin, Y. Skhiri, J. C. Baret, D. Le Corre, L. Mazutis, C. B. Salem, F. Millot, A. El Harrak, J. B. Hutchison, J. W. Larson, D. R. Link, P. Laurent-Puig, A. D. Griffiths, V. Taly, *Lab Chip* **2011**, *11*, 2156; c) F. Schuler, M. Trotter, M. Geltman, F. Schwemmer, S. Wadle, E. Dominguez-Garrido, M. Lopez, C. Cervera-Acedo, P. Santibanez, F. von Stetten, R. Zengerle, N. Paust, *Lab Chip* **2016**, *16*, 208.
- [3] a) J. Clausell-Tormos, D. Lieber, J. C. Baret, A. El-Harrak, O. J. Miller, L. Frenz, J. Blouwolf, K. J. Humphry, S. Koster, H. Duan, C. Holtze, D. A. Weitz, A. D. Griffiths, C. A. Merten, *Chem. Biol.* **2008**, *15*, 427; b) S. Koster, F. E. Angile, H. Duan, J. J. Agresti, A. Wintner, C. Schmitz, A. C. Rowat, C. A. Merten, D. Pisignano, A. D. Griffiths, D. A. Weitz, *Lab Chip* **2008**, *8*, 1110; c) T. Beneyton, S. Thomas, A. D. Griffiths, J. M. Nicaud, A. Drevelle, T. Rossignol, *Microb. Cell Fact.* **2017**, *16*, 18.
- [4] a) T. M. Squires, S. R. Quake, *Rev. Mod. Phys.* **2005**, *77*, 977; b) Y. Liu, X. Jiang, *Lab Chip* **2017**, *17*, 3960.
- [5] J. C. McDonald, G. M. Whitesides, *Acc. Chem. Res.* **2002**, *35*, 491.
- [6] a) A. I. Shalhan, P. Smejkal, M. Corban, R. M. Guijt, M. C. Breadmore, *Anal. Chem.* **2014**, *86*, 3124; b) C. M. Ho, S. H. Ng, K. H. Li, Y. J. Yoon, *Lab Chip* **2015**, *15*, 3627.
- [7] a) R. Walczak, K. Adamski, *J. Micromech. Microeng.* **2015**, *25*, 085013; b) N. P. Macdonald, J. M. Cabot, P. Smejkal, R. M. Guijt, B. Paull, M. C. Breadmore, *Anal. Chem.* **2017**, *89*, 3858.
- [8] a) P. J. Kitson, M. H. Rosnes, V. Sans, V. Dragone, L. Cronin, *Lab Chip* **2012**, *12*, 3267; b) T. Baden, A. M. Chagas, G. J. Gage, T. C. Marzullo, L. L. Prieto-Godino, T. Euler, *PLoS Biol.* **2015**, *13*, e1002086; c) S. Waheed, J. M. Cabot, N. P. Macdonald, T. Lewis, R. M. Guijt, B. Paull, M. C. Breadmore, *Lab Chip* **2016**, *16*, 1993.
- [9] a) F. Li, N. P. Macdonald, R. M. Guijt, M. C. Breadmore, *Anal. Chem.* **2017**, *89*, 12805; b) A. Enders, I. G. Siller, K. Urmann, M. R. Hoffmann, J. Bahnemann, *Small* **2019**, *15*, e1804326.
- [10] F. Li, N. P. Macdonald, R. M. Guijt, M. C. Breadmore, *Anal. Chem.* **2019**, *91*, 1758.
- [11] F. Li, P. Smejkal, N. P. Macdonald, R. M. Guijt, M. C. Breadmore, *Anal. Chem.* **2017**, *89*, 4701.
- [12] A. J. Morgan, L. Hidalgo San Jose, W. D. Jamieson, J. M. Wymant, B. Song, P. Stephens, D. A. Barrow, O. K. Castell, *PLoS One* **2016**, *11*, e0152023.
- [13] a) S. Tsuda, H. Jaffery, D. Doran, M. Hezwani, P. J. Robbins, M. Yoshida, L. Cronin, *PLoS One* **2015**, *10*, e0141640; b) J. M. Zhang, E. Q. Li, A. A. Aguirre-Pablo, S. T. Thoroddsen, *RSC Adv.* **2016**, *6*, 2793.
- [14] H. Gong, B. P. Bickham, A. T. Woolley, G. P. Nordin, *Lab Chip* **2017**, *17*, 2899.
- [15] H. Gong, M. Beauchamp, S. Perry, A. T. Woolley, G. P. Nordin, *RSC Adv.* **2015**, *5*, 106621.
- [16] M. J. Beauchamp, H. Gong, A. T. Woolley, G. P. Nordin, *Micromachines* **2018**, *9*, 326.
- [17] a) S. Vijayan, M. Hashimoto, *RSC Adv.* **2019**, *9*, 2822; b) C. Martino, S. Berger, R. C. Wootton, A. J. deMello, *Lab Chip* **2014**, *14*, 4178.
- [18] J. M. Zhang, A. A. Aguirre-Pablo, E. Q. Li, U. Buttner, S. T. Thoroddsen, *RSC Adv.* **2016**, *6*, 81120.
- [19] S. K. Anciaux, M. Geiger, M. T. Bowser, *Anal. Chem.* **2016**, *88*, 7675.
- [20] M. Mannel, L. Selzer, R. Bernhardt, J. Thiele, *Adv. Mater. Technol.* **2019**, *4*, 1800408.

- [21] R. Yuan, M. B. Nagarajan, J. Lee, J. Voldman, P. S. Doyle, Y. Fink, *Small* **2018**, *14*, 1803585.
- [22] G. D. Hoople, D. A. Rolfe, K. C. McKinstry, J. R. Noble, D. A. Dornfeld, A. P. Pisano, *J. Micro Nano-Manuf.* **2014**, *2*, 034502.
- [23] S. Moylan, A. Cooke, K. Jurrens, J. Slotwinski, M. A. Donmez, presented at *Proceedings National Institute of Standards and Technology (NIST)*, Gaithersburg, MD, May **2012**.
- [24] S. Moylan, D. Blumenfeld, M. McGlaulin, R. Fesperman, M. Donmez, in *Evaluation of proposed test artifacts for five-axis machine tools, Proceedings - ASPE 2011 Annual Meeting*, American Society for Precision Engineering, Denver, Colorado **2011**, p. 520–523.
- [25] W. Lee, L. M. Walker, S. Anna, *Phys. Fluids* **2009**, *21*, 032103.
- [26] S. Moylan, J. Slotwinski, A. Cooke, K. Jurrens, M. A. Donmez, in *Solid Freeform Fabrication Symp. Proceedings*, University of Texas, Austin **2012**, p. 902.
- [27] G. I. Salentijn, P. E. Oomen, M. Grajewski, E. Verpoorte, *Anal. Chem.* **2017**, *89*, 7053.
- [28] P. H. King, G. Jones, H. Morgan, M. R. de Planque, K. P. Zauner, *Lab Chip* **2014**, *14*, 722.
- [29] A. Waldbaur, H. Rapp, K. Länge, B. E. Rapp, *Anal. Methods* **2011**, *3*, 2681.
- [30] a) G. Comina, A. Suska, D. Filippini, *Lab Chip* **2014**, *14*, 424; b) A. Bonyar, H. Santha, M. Varga, B. Ring, A. Vitez, G. Harsanyi, *Int. J. Mater. Form.* **2014**, *7*, 189.
- [31] T. S. Kaminski, O. Scheler, P. Garstecki, *Lab Chip* **2016**, *16*, 2168.
- [32] a) J. C. Baret, O. J. Miller, V. Taly, M. Ryckelynck, A. El-Harrak, L. Frenz, C. Rick, M. L. Samuels, J. B. Hutchison, J. J. Agresti, D. R. Link, D. A. Weitz, A. D. Griffiths, *Lab Chip* **2009**, *9*, 1850; b) R. Obexer, A. Godina, X. Garrabou, P. R. Mittl, D. Baker, A. D. Griffiths, D. Hilvert, *Nat. Chem.* **2017**, *9*, 50.
- [33] F. Gielen, R. Hours, S. Emond, M. Fischlechner, U. Schell, F. Hollfelder, *Proc. Natl. Acad. Sci. USA* **2016**, *113*, E7383.
- [34] P. Y. Colin, B. Kintsjes, F. Gielen, C. M. Miton, G. Fischer, M. F. Mohamed, M. Hyvonen, D. P. Morgavi, D. B. Janssen, F. Hollfelder, *Nat. Commun.* **2015**, *6*, 10008.
- [35] a) B. L. Wang, A. Ghaderi, H. Zhou, J. Agresti, D. A. Weitz, G. R. Fink, G. Stephanopoulos, *Nat. Biotechnol.* **2014**, *32*, 473; b) S. L. Sjoström, Y. Bai, M. Huang, Z. Liu, J. Nielsen, H. N. Joensson, H. Andersson Svahn, *Lab Chip* **2014**, *14*, 806.
- [36] a) D. A. Siegele, J. C. Hu, *Proc. Natl. Acad. Sci. USA* **1997**, *94*, 8168; b) J. A. Megerle, G. Fritz, U. Gerland, K. Jung, J. O. Radler, *Biophys. J.* **2008**, *95*, 2103.
- [37] A. Autour, M. Ryckelynck, *Micromachines* **2017**, *8*, 128.
- [38] a) J. Stegmaier, R. Alshut, M. Reischl, R. Mikut, *Biomed. Eng.* **2012**, *57*, 458; b) R. Mikut, A. Bartschat, W. Doneit, J. Ordiano, B. Schott, J. Stegmaier, S. Waczowicz, M. Reischl, *The MATLAB Toolbox SciXMiner: User's Manual and Programmer's Guide*, arXiv:1704.03298, **2017**.
- [39] a) H. S. Rho, A. T. Hanke, M. Ottens, H. Gardeniers, *PLoS One* **2016**, *11*, e0153437; b) N. Rupcich, J. D. Brennan, *Anal. Chim. Acta* **2003**, *500*, 3.
- [40] A. Fallah-Araghi, K. Meguellati, J.-C. Baret, A. E. Harrak, T. Mangeat, M. Karplus, S. Ladame, C. M. Marques, A. D. Griffiths, *Phys. Rev. Lett.* **2014**, *112*, 028301.
- [41] C. Barner-Kowollik, M. Bastmeyer, E. Blasco, G. Delaittre, P. Müller, B. Richter, M. Wegener, *Angew. Chem., Int. Ed.* **2017**, *56*, 15828.
- [42] Y. Jia, Y. Ren, L. Hou, W. Liu, X. Deng, H. Jiang, *Small* **2017**, *13*, 1702188.
- [43] D. G. Gibson, L. Young, R. Y. Chuang, J. C. Venter, C. A. Hutchison 3rd, H. O. Smith, *Nat. Methods* **2009**, *6*, 343.